18 October 2002

NEER Grant: DE-FG07-98ID13632
Final report

Title: Reactor whole core transport calculations without fuel assembly homogenization

Investigator: Nicholas Tsoulfanidis, University of Missouri-Rolla
Co-Investigator: Elmer Lewis, Northwestern University

Funding period: 9-1-98 to 8-31-01

General Objective: Numerical algorithms developed to serve as the basis for the next generation of computer codes to perform accurate 3D core physics calculations.

The two-dimensional form of a finite element formulation of VARIANT has been refined to accept higher order angular approximations and more elaborate finite element representations in 2 and 3D formulations.

Papers presented in national and international meetings, based on this grant:

1. "Whole –core neutron transport calculations without cross section homogenization", Proceedings ICONE 8 International conference on Nuclear Engineering, April 2-6, 2000, Baltimore, MD, USA.

2. "Whole-core neutron transport calculations without fuel-coolant homogenization", PHYSOR-2000, Pittsburgh, PA, USA.

3. " Neutron transport validation of variational nodal subelement methods", Proc. Fourth Int. Conf. Supercomputing in Nuclear Applications, Tokyo, Sept. 4-7, 2000, SNA-2000.

4. " Comparison of angular approximations for PWR cell calculations", ANS Trans., 84, p.90, June 2001.

5. " A finite subelement generalization of the variational nodal method"
(see attachments)
Paper to be published in Nuclear Science & Engineering. Dr. Mike Smith received the American Nuclear Society Mark Mills award for this work. Dr. Smith, who was supported by this contract, is now on the staff of Argonne National Laboratory doing research in reactor physics and computational methods development. As a result of his work there now exist at ANL a prototypical form of the VARIANT code that utilizes the subelement methods developed in his

thesis. Consideration is being given into possible approaches for incorporating the subelement approach into the production version of the VARIANT code.

Also based on the Grant:

MS Thesis of M. Smith " Implementation of the finite element method in a nodal transport program to allow for heterogeneous geometries", May 2000

Ph. D., Dissertation of M. Smith, " A 3-D nodal neutron transport program with the ability to handle spatial heterogeneities", October 2001.

Benchmark problem participation: NEA Benchmark on deterministic 2-D/3-D MOX fuel assembly transport calculations without spatial homogenization (C5G7 MOX).

A Finite Subelement Generalization of the Variational Nodal Method

M. A. Smith*, N. Tsoulfanidis
University of Missouri, Rolla
Department of Nuclear Engineering
Rolla, Missouri 65409

E. E. Lewis
Northwestern University
Department of Mechanical Engineering
Evanston, Illinois 60208

G. Palmiotti & T. A. Taiwo
Argonne National Laboratory
9700 South Cass Avenue
Argonne, Illinois 60439

Abstract--*The variational nodal method is generalized by dividing each spatial node into a number of triangular finite elements designated as subelements. The finite subelement trial functions allow for explicit geometry representations within each node, thus eliminating the need for nodal homogenization. The method is implemented within the Argonne National Laboratory code VARIANT and applied to two-dimensional multigroup problems.*

Eigenvalue and pin-power results are presented for a four-assembly OECD/NEA benchmark problem containing enriched UO_2 and MOX fuel pins. Our seven-group model combines spherical or simplified spherical harmonic approximations in angle with isoparametric linear or quadratic subelement basis functions, thus eliminating the need for fuel-coolant homogenization. Comparisons with reference seven-group Monte Carlo solutions indicate that in the absence of pin-cell homogenization, high-order angular approximations are required to obtain accurate eigenvalues, while the results are substantially less sensitive to the refinement of the finite subelement grids.

I. INTRODUCTION

Nodal diffusion methods have been widely employed for performing whole-core reactor physics calculations.[1] More recently, nodal transport methods have found increased use in treating problems where steep flux gradients, sharp cross section discontinuities, and other phenomena lead to substantial inaccuracies in the diffusion approximation.[2,3] In particular, the variational nodal method incorporated in the Argonne

* Now At Argonne National Laboratory

National Laboratory code VARIANT[4,5] performs multigroup spherical harmonics (P_N) or simplified spherical harmonics (SP_N) calculations in two- and three-dimensional Cartesian and hexagonal geometries.[5-7]

Nodal codes, including VARIANT, typically utilize homogenized cross sections for fuel assembly-size nodes. With whole-core transport methods available, the largest remaining uncertainties most frequently revolve around the use of these homogenized cross sections and the subsequent dehomogenization procedures needed to reconstruct fuel pin powers. Despite the use of high-order angular approximations in whole-core transport calculations, the homogenization approximations still cast doubt on the accuracy of the results. To eliminate the need for homogenized nodes, we have derived a subelement formulation of the variational nodal method. In VARIANT, the even-parity transport equation is solved within each node and the nodes are coupled together by odd-parity Lagrange multipliers. The generalized method presented here retains the multigroup response matrix formalism in VARIANT coupled with P_N or SP_N angular approximations. However, the polynomial trial functions previously used to represent the spatial flux distribution within the node are replaced by finite elements with continuous, piecewise polynomial trial functions. This approach allows the cross sections to be discontinuous at the finite element interfaces within each node, thus the requirement that the nodes be homogeneous is eliminated. We have chosen to designate these finite elements as subelements, since the variational nodal method itself may be viewed as a hybrid finite element formulation.[8]

An earlier investigation implemented square subelements with piecewise bilinear trial functions, allowing homogenized fuel pin-cells to be represented explicitly within a fuel assembly-size node.[8] Increasingly, however, advances in computing power have allowed such problems to be treated such that each node is the size of one homogenized fuel pin-cell. In this work we implement triangular isoparametric subelement approximations of a heterogeneous pin-cell geometry where the interface between the fuel and coolant within each node is explicitly represented; the fuel, gap, and cladding remain homogenized. In Sec. II, the subelement theory is presented while in Sec. III the generalized formulation is applied to a two-dimensional benchmark problem, and its capabilities and limitations are discussed.

II. THEORY

Since the variational nodal method utilizes a standard multigroup formulation, we take the within-group transport equation as the starting point for our derivations

$$\hat{\Omega}\cdot\vec{\nabla}\psi(\vec{r},\hat{\Omega})+\Sigma_t(\vec{r})\psi(\vec{r},\hat{\Omega})=\Sigma_s(\vec{r})\phi(\vec{r})+S(\vec{r}), \qquad (1)$$

where for this work we assume isotropic scattering and sources. In Eq. (1), $\psi(\vec{r},\hat{\Omega})$ and $\phi(\vec{r})$ represent the group angular and scalar flux, $S(\vec{r})$ is the group source, and $\Sigma_t(\vec{r})$ and $\Sigma_s(\vec{r})$ are the total and within-group scattering cross sections. We can transform Eq. (1) into a second-order even-parity form yielding

$$\hat{\Omega}\cdot\nabla\Sigma_t^{-1}\hat{\Omega}\cdot\vec{\nabla}\psi^+(\vec{r},\hat{\Omega})+\Sigma_t\psi^+(\vec{r},\hat{\Omega})=\Sigma_s\phi(\vec{r})+S(\vec{r}), \qquad (2)$$

where the even- and odd-parity flux components are defined by

$$\psi^{\pm}(\vec{r},\hat{\Omega}) = \frac{1}{2}\left[\psi(\vec{r},\hat{\Omega}) \pm \psi(\vec{r},-\hat{\Omega})\right]. \tag{3}$$

We next write Eq. (2) in a functional form with odd-parity boundary conditions,

$$\begin{aligned} F\left[\psi^{+},\psi^{-}\right] = \int dV \int d\Omega \left[\Sigma_t^{-1}\left(\hat{\Omega}\cdot\vec{\nabla}\psi^{+}\right)^2 + \psi^{+}\Sigma_t\,\psi^{+}\right] - \int dV\left(\phi\,\Sigma_s\phi + 2\phi S\right) \\ +2\int d\Gamma \int d\Omega \hat{\Omega}\cdot\hat{n}\,\psi^{+}\psi^{-} \end{aligned} \tag{4}$$

where V is the problem domain, bounded by the surface Γ with outward normal $\hat{n}$.

To obtain the nodal functional, we decompose the problem domain into subdomains V_v (called nodes) and define the odd-parity flux $\psi^{-}(\vec{r},\hat{\Omega})$ on the surfaces, Γ_γ, of each node. Using these definitions, we can rewrite Eq. (4) as a superposition of nodal contributions:

$$F\left[\psi^{+},\psi^{-}\right] = \sum_v F_v\left[\psi^{+},\psi^{-}\right], \tag{5}$$

where the nodal functional is written as

$$\begin{aligned} F_v\left[\psi^{+},\psi^{-}\right] = \int dV \int d\Omega \left[\Sigma_t^{-1}\left(\hat{\Omega}\cdot\vec{\nabla}\psi^{+}\right)^2 + \psi^{+}\Sigma_t\,\psi^{+}\right] - \int dV\left[\phi\,\Sigma_s\phi + 2\phi S\right] \\ +2\int d\Gamma \int d\Omega \left[\hat{\Omega}\cdot\hat{n}\,\psi^{+}\psi^{-}\right] \end{aligned} . \tag{6}$$

The inclusion of the Lagrange multipliers for $\psi^{-}(\vec{r},\hat{\Omega})$ allows the use of $\psi^{+}(\vec{r},\hat{\Omega})$ trial functions that are discontinuous across the nodal interfaces. The trial functions for $\psi^{-}(\vec{r},\hat{\Omega})$, of course, are uniquely defined along the interfaces.

To implement the subelement treatment, we subdivide the nodal volume into triangular isoparametric finite elements as seen in Fig. (1), where L and Q indicate elements with linear and quadratic basis functions, respectively. The nodal functional from Eq. (6) is now written as a superposition of subelement functionals

$$F_v\left[\psi^{+},\psi^{-}\right] = \sum_e F_{(e)}\left[\psi_e^{+},\psi^{-}\right], \tag{7}$$

where the functional for each subelement volume V_e, is given as

$$\begin{aligned} F_{(e)}\left[\psi_e^{+},\psi^{-}\right] = \int_{(e)} dV \int d\Omega \left[\Sigma_{t,e}^{-1}\left(\hat{\Omega}\cdot\vec{\nabla}\psi_e^{+}\right)^2 + \psi_e^{+}\Sigma_{t,e}\,\psi_e^{+}\right] \\ -\int_{(e)} dV\left[\phi_e\,\Sigma_{s,e}\phi_e + 2\phi_e S_e\right] + 2\int_{(e)} d\Gamma \int d\Omega \hat{\Omega}\cdot\hat{n}\,\psi_e^{+}\psi^{-} \end{aligned} . \tag{8}$$

In this work we consider only finite element basis functions that are continuous across subelement interfaces. Since continuous trial functions are used within each node, the surface term in Eq. (8) appears only along the nodal interfaces, and thus only for those subelements adjacent to nodal interfaces.

Within each subelement the spatial and angular approximation of the even parity flux is given by

$$\psi_e^{+}\left(\vec{r},\hat{\Omega}\right) = \mathbf{g}^T(\hat{\Omega}) \otimes \mathbf{f}^T(\vec{r})\,\xi_e, \qquad \vec{r} \in V_e \tag{9}$$

the source is given by

$$S_e\left(\vec{r}\right) = \mathbf{f}^T(\vec{r})\,\mathbf{s}_e, \tag{10}$$

and the approximation of the odd-parity flux along each nodal interface γ is given by

$$\psi^{-}\left(\vec{r},\hat{\Omega}\right)=\mathbf{k}_{\gamma}^{T}(\hat{\Omega})\otimes\mathbf{h}_{\gamma}^{T}(\vec{r})\,\chi_{\gamma}. \qquad \vec{r}\in\Gamma_{\gamma} \tag{11}$$

Here the symbol $\otimes$ indicates Kronecker tensor multiplication of the angular and spatial trial functions, and ξ_e and χ_γ are the unknown coefficients. The even- and odd-parity angular functions $\mathbf{g}(\hat{\Omega})$ and $\mathbf{k}_\gamma(\hat{\Omega})$ are vectors of spherical harmonics defined such that Rumyantsev boundary conditions are satisfied across the nodal interfaces.[6,9] The spatial dependence, $\mathbf{h}_\gamma(\vec{r})$, of the odd-parity Lagrange multiplier is approximated with a set of orthogonal polynomials previously used in VARIANT.[4] The spatial distribution of the even-parity flux, $\mathbf{f}(\vec{r})$, is given by the finite element trial functions, the cross sections are assumed to be unique constants within each finite element.

Inserting Eqs. (9), (10) and (11) into Eq. (8) yields the algebraic functional for each subelement

$$\begin{aligned} F_e\left[\xi_e,\chi_\gamma\right]=\xi_e^T\left(\sum_{K,L}\mathbf{H}^{K,L}\otimes\Sigma_{t,e}^{-1}\mathbf{P}^{K,L,e}+\mathbf{I}\otimes\Sigma_{t,e}\mathbf{F}^e-\mathbf{K}\otimes\Sigma_{s,e}\mathbf{F}^e\right)\xi_e \\ -2\xi_e^T\left(\mathbf{K}\otimes\mathbf{F}^e\mathbf{s}_e\right)+2\sum_{\gamma'}\xi_e^T\left(\mathbf{E}_{\gamma'}\otimes\mathbf{D}_{\gamma'}^e\right)\chi_{\gamma'} \end{aligned} \tag{12}$$

where the spatial integrations over each subelement result in the matrices

$$P_{i,j,e}^{K,L}=\int_e dV\left[\vec{\nabla}_K f_i(\vec{r})\vec{\nabla}_L f_j(\vec{r})\right] \tag{13}$$

$$F_{i,j}=\int_e dV\left[f_i(\vec{r})f_j(\vec{r})\right], \tag{14}$$

and

$$D_{\gamma,i,j}^e=\int_{\gamma,e}dA\left[f_i(\vec{r})h_j(\vec{r})\right]. \tag{15}$$

The angular integrations yield the matrices

$$H_{m,n}^{K,L}=\int d\Omega\left[\hat{\Omega}^K g_m\left(\hat{\Omega}\right)\hat{\Omega}^L g_n\left(\hat{\Omega}\right)\right], \tag{16}$$

$$I_{m,n}=\int d\Omega\left[g_m\left(\hat{\Omega}\right)g_n\left(\hat{\Omega}\right)\right]=\delta_{m,n}, \tag{17}$$

$$K_m=\int d\Omega\left[g_m\left(\hat{\Omega}\right)\right]=\delta_{m,1}, \tag{18}$$

and

$$E_{\gamma,m,n}=\int d\Omega\left[\hat{\Omega}\cdot n_\gamma\, g_m\left(\hat{\Omega}\right)k_n\left(\hat{\Omega}\right)\right], \tag{19}$$

which have the same form as those previously used in VARIANT.[4]

To assemble the nodal functional we must map the local finite element trial function coefficients, ξ_e, into a nodal vector of coefficients ζ. This is accomplished with a Boolean transformation matrix Ξ_e.

$$\xi_e=\Xi_e\zeta. \tag{20}$$

The Boolean transformation, a description of which can be found in finite element literature,[10] is the mechanism by which continuity is enforced across subelement interfaces.

The introduction of Eq. (20) into Eq. (12) and subsequent substitution into Eq. (7) yields

$$F_v[\zeta,\chi] = \zeta^T \mathbf{A}\zeta - 2\zeta^T \mathbf{s} + 2\sum_{\gamma'} \zeta^T \mathbf{M}_{\gamma'} \chi_{\gamma'}, \tag{21}$$

where

$$\mathbf{A} = \sum_{K,L} \mathbf{H}^{K,L} \otimes \sum_e \Xi_e^T \Sigma_{t,e}^{-1} \mathbf{P}^{K,L,e} \Xi_e + \mathbf{I} \otimes \sum_e \Xi_e^T \Sigma_{t,e} \mathbf{F}^e \Xi_e - \mathbf{K} \otimes \sum_e \Xi_e^T \Sigma_{s,e} \mathbf{F}^e \Xi_e, \tag{22}$$

$$\mathbf{s} = \mathbf{K} \otimes \sum_e \Xi_e^T \mathbf{F}^e \mathbf{s}_e \Xi_e, \tag{23}$$

$$\mathbf{M}_\gamma = \mathbf{E}_\gamma \otimes \sum_e \Xi_e^T \mathbf{D}_\gamma^e, \tag{24}$$

and $\mathbf{I}$ is the identity matrix.

With the treatment of the spatial and angular approximations within each node completed, we may now proceed to the response matrix formulation. We first require the functional to be stationary with respect to arbitrary variations in the vectors of unknown coefficients. Upon taking the variation of Eq. (21) with respect to the even-parity flux coefficients, ζ, we obtain

$$\mathbf{A}\zeta - \mathbf{s} + \sum_{\gamma'} \mathbf{M}_{\gamma'} \chi_{\gamma'} = 0, \tag{25}$$

which may be solved for ζ to yield

$$\zeta = \mathbf{A}^{-1}\mathbf{s} - \sum_{\gamma'} \mathbf{A}^{-1}\mathbf{M}_{\gamma'} \chi_{\gamma'}. \tag{26}$$

We next sum Eq. (21) over all of the nodes, as indicated in Eq. (5), and require the resulting functional to be stationary with respect to variations in the Lagrange multiplier coefficients χ_γ thereby restricting

$$\varphi_\gamma = \mathbf{M}_\gamma^T \zeta \tag{27}$$

to be continuous across nodal interfaces.

We can merge Eq. (27) with Eq. (26) to obtain

$$\varphi_\gamma = \mathbf{M}_\gamma^T \mathbf{A}^{-1}\mathbf{s} - \sum_{\gamma'} \mathbf{M}_{\gamma'}^T \mathbf{A}^{-1}\mathbf{M}_{\gamma'} \chi_{\gamma'}, \tag{28}$$

which can further be partitioned with respect to nodal interfaces to obtain

$$\varphi = \mathbf{M}^T \mathbf{A}^{-1}\mathbf{s} - \mathbf{M}^T \mathbf{A}^{-1}\mathbf{M}\chi. \tag{29}$$

To arrive at the final response matrix form we make a change of variables and introduce the partial current-like variables

$$\mathbf{j}^{\pm} = \tfrac{1}{4}\varphi \pm \tfrac{1}{2}\chi \tag{30}$$

along the node interfaces. Combining Eqs. (29) and (30) we get the response matrix equation

$$\mathbf{j}^{+} = \mathbf{R}\mathbf{j}^{-} + \mathbf{B}\mathbf{s}, \tag{31}$$

where we have made use of the intermediate matrices

$$\mathbf{R} = \left(\tfrac{1}{2}\mathbf{M}^{\mathbf{T}}\mathbf{A}^{-1}\mathbf{M} + \mathbf{I}\right)^{-1}\left(\tfrac{1}{2}\mathbf{M}^{\mathbf{T}}\mathbf{A}^{-1}\mathbf{M} - \mathbf{I}\right), \tag{32}$$

$$\mathbf{B} = \left(\tfrac{1}{2}\mathbf{M}^{\mathbf{T}}\mathbf{A}^{-1}\mathbf{M} + \mathbf{I}\right)^{-1}\left(\tfrac{1}{2}\mathbf{M}^{\mathbf{T}}\mathbf{A}^{-1}\right), \tag{33}$$

and the identity matrix $\mathbf{I}$.

An additional approximation implemented in conjunction with the subelement approximation is source lumping. Instead of using a consistent source, as that defined by Eq. (10), the source is lumped or averaged over several contiguous elements containing

identical cross sections.[11] Source lumping has two major benefits: the number of source components is reduced, thus reducing the computational burden of the fission source iterations, and the lumped source components converge much faster than the consistent source.

III. RESULTS

VARIANT has been modified to accommodate the subelement formulation and employed to solve a two-dimensional benchmark problem specified by OECD/NEA.[12] This benchmark problem was formulated to test the accuracy of the space-angle approximations implemented in deterministic transport codes. The core configuration for the benchmark problem is shown in Fig. 2, where each fuel pin is 1.08 cm in diameter, each square is 1.26 cm in length, and the moderator region is 21.42 cm thick. Included in the benchmark specification are seven-group cross sections for each of the compositions defined in Fig. 2. For comparison, a reference multigroup Monte Carlo solution was obtained for the steady state eigenvalue and pin power distribution. To estimate the importance of the spatial and angular approximations for the benchmark, we first examine approximations of several single pin-cell geometries and then apply a subset of these approximations to the benchmark.

III.A Pin-cell Results

For this work we chose the node size to correspond to a single pin-cell and made use of the triangular finite element representations of the pin-cell geometry given in Fig. 1 (fuel region is shaded). In each of the finite element meshes the fuel/coolant volume ratio is exactly maintained. As indicated by Fig. 1, the quadratic meshes (Q) allow for a more faithful representation of the fuel-coolant interface than the linear meshes (L). To assess the sensitivity to the finite element mesh refinements and to refinements of the angular approximation, we solved several single pin-cell problems with reflected boundary conditions using the benchmark cross-sections. For brevity, we display the eigenvalue results only for the highest enrichment MOX fuel pin-cell problem; this pin-cell yielded the largest errors when low-order space-angle approximations were employed.

A reference eigenvalue solution for the high-enriched MOX fuel pin-cell problem was obtained with the Monte Carlo code MCNP[13] and a comparative solution obtained with the collision probability code DRAGON.[14] The MCNP reference eigenvalue was found to be 1.17472±0.00016 (99% confidence interval) and the best collision probability eigenvalue solution was 1.17508. VARIANT was used to obtain eigenvalue solutions of the pin-cell problem using a consistent source approximation and exact boundary conditions (i.e. without Lagrange multiplier approximations). The finite element mesh solutions for P_N and SP_N angular approximations are plotted in Figs. 3 and 4, respectively, along with the reference MCNP solution.

The eigenvalue results indicate that the largest errors arise from the angular approximations. For a given order N, the P_N and SP_N results are quite close to each other, but both converge very slowly toward the Monte Carlo solution. The P_N results should converge to the Monte Carlo result and more detailed studies[11] have shown that angular expansions as high as P_{31} are required. Higher order P_N cell calculations are not included

in this work, since P_{15} corresponds to the maximum order that can presently be applied in the variational nodal framework to the OECD/NEA benchmark problem. Unlike the P_N approximation, the SP_N approximation can be applied with very high orders. However, Fig. 4 indicates that the SP_N approximation does not produce accurate results. The residual eigenvalue error observed in Fig. 4 is not unexpected since the SP_N treatment is not a rigorous treatment of the angular variable, and thus cannot be expected to produce exact solutions for transport problems.

In contrast to the angular approximation, the convergence with respect to spatial mesh refinement is quite rapid as indicated by Figs. 3 and 4. With both the P_N and SP_N treatments, the spatial approximation appears to be sufficiently converged using the Q3 mesh. The large differences between the solutions using linear or quadratic finite element meshes is attributable to quadratic meshes giving $O(h^4)$ accuracy and linear meshes giving $O(h^2)$ accuracy. Consequently, for the benchmark problem, we employ quadratic spatial mesh approximations. Specifically, we choose to use the Q2 mesh since the difference between the Q2 and the Q3 mesh was found to be relatively minute when compared to the errors caused by the angular approximation.

III.B Benchmark Problem Results

To employ the formalism of Sec. II, two additional approximations are applied to solve the OECD/NEA benchmark problem. First, Lagrange multipliers (low order polynomials) are used to approximate the spatial distribution of the odd-parity flux along the nodal interfaces. Second, the group sources, defined to be consistent with the finite subelement basis functions, are simplified by averaging over 2, 5, or 8 sub-regions of each pin-cell as indicated by Fig. 5. Combined, these two approximations substantially reduce the computational effort, while resulting in minor losses in accuracy of both the eigenvalue and pin power solution.

Figure 6 compares Q2 mesh, quadratic Lagrange multiplier, 8 lumped source, P_N and SP_N eigenvalue solutions for the OECD/NEA benchmark problem along with the eigenvalue solutions for the infinite-lattice UO_2 pin-cell and the highest enrichment MOX pin-cells. The 99% confidence intervals on the Monte Carlo eigenvalue solutions for the OECD/NEA benchmark problem, the UO_2 pin-cell, and the MOX pin-cell are 1.18655±0.008%, 1.32557±0.07%, and 1.17472±0.03%, respectively. As seen in Fig. 6, the benchmark eigenvalue is an amalgamation of the individual pin-cell problems; additional calculations have shown that the lower enrichment MOX pin-cells behave similarly to the highest enrichment MOX pin-cell, but with a smaller error in the diffusion solution.[11] The P_N solutions indicate convergence towards the Monte Carlo solution, but memory requirements and computational times prohibit the use of a high enough angular approximation to achieve asymptotic convergence. Since two-dimensional P_N approximations require $(N+1)^2/4$ even-parity angular basis functions while SP_N require only $(N+1)/2$, much higher order SP_N approximations can be applied. However, substantial residual error exists in the eigenvalue solution when using the SP_N approximation.

Most apparent from Fig. 6 is that the transport errors incurred in the angular variables at the lattice-cell level dominate the global eigenvalue results. In contrast to the heterogeneous pin-cell model, the use of pin-cell homogenized cross sections, obtained

from the lattice code DRAGON and employed in the standard version of VARIANT, show little difference between a P_3 and P_5 approximation. Furthermore, the P_5 eigenvalue solution is only 0.127% in error of the reference solution. This seemingly advantageous aspect of using the homogenous treatment does not carry over to the accuracy of the pin power distribution.

Tables I and II display pin power and eigenvalue results for P_N and SP_N approximations, respectively, both using a quadratic Lagrange multiplier approximation and an 8 lumped source approximation. The results of the P_5 homogenized pin-cell treatment and the 99% confidence intervals for the Monte Carlo solution are also included for comparison. For each result, three measures of the pin power error are given along with the eigenvalue percent error: the percent error in the pin with the maximum power, the absolute value of the maximum percent error anywhere in the fuel assemblies, and the root mean squared (RMS) percent error for the pin power distribution.

As in Fig. 6, the eigenvalue error in Tables I and II decreases monotonically with an increasing P_N approximation, but the pin power errors show no such systematic improvement for an angular approximation of P_7 or greater. Such seemingly erratic behavior can be traced to a complex pattern of error cancellation between, angular, subelement, lumped source, and nodal interface approximations. To resolve this effect we include Q2 mesh results using a consistent source and quadratic Lagrange multiplier approximation in Table III, and results using a consistent source and a cubic Lagrange multiplier in Table IV. We also include a Q2 mesh SP_{25} solution in Table IV using a consistent source and cubic Lagrange multiplier approximation for further comparison to the SP_N approximation.

Both Tables III and IV have eigenvalue solutions that are comparable to those given in Table I, but the pin power solutions display a more monotonic behavior. A direct comparison of Table I to Table III shows that with a consistent source approximation the pin power results converge monotonically towards the reference solution through P_9 as opposed to a P_5 approximation seen in Table I. The introduction of the consistent source removes entirely the errors introduced by the lumped source approximation and demonstrates that the lack of monotonic convergence is attributable in large part to cancellation of error between the angular approximation and the lumped source approximation. In Table IV, monotonic convergence of both the eigenvalue and pin power solutions is evident through the P_{13} solution, indicating that refinement of the Lagrange multiplier approximation is also necessary to completely resolve the inconsistent convergence behavior observed in Table I. Further improvements from calculations using quadric Lagrange multiplier approximations were found to be negligible. Comparison of the SP_N solution in Table IV to those of Table II demonstrates that the errors resulting from spatial approximations are small compared with those introduced by the inability of SP_N approximations to approach asymptotically the exact solution of the transport equation.

In summary, Tables II and IV show that the errors in the pin power distribution for SP_N solutions are substantially larger than those of the P_N solutions in Tables I, II, and III. Moreover, the homogenous pin-cell treatment also results in solutions more accurate than the SP_N heterogeneous solutions, reaffirming that the SP_N approximation is not an adequate approach to solving this problem. More importantly, the errors for the P_N solutions utilizing heterogeneous pin-cell cross sections are substantially smaller than

those using the homogenous pin-cell cross sections. Thus, although the homogenous approach is computationally faster, the inclusion of cell heterogeneities results in a more accurate representation of the pin power distribution.

IV. CONCLUSIONS

Two significant tasks have been accomplished. First, the finite subelement formulation has been implemented in VARIANT to treat heterogeneous nodes in two-dimensional Cartesian geometries. Implementation of the subelement formulation to treat heterogeneous nodes in three-dimensional Cartesian in addition to further refinements of the angular approximation are ongoing. Second, the heterogeneous node formulation has been employed to compute the eigenvalue and power distribution for a MOX benchmark problem that combines strong lattice effects with sharp spatial gradients throughout the problem geometry. These calculations, in which the node consists of a single fuel pin-cell with no fuel-coolant homogenization, are computationally intensive. For while we found that convergence of the solutions is rapid with respect to the spatial subelement grid, very high order spherical harmonic approximations are required to obtain accurate eigenvalue and pin power solutions.

Improved computational algorithms presently under study should result in significant computational time reductions for water reactor lattice problems similar to the benchmark presented here. If larger nodes are utilized, nodes that contain several pin-cells for example, the computational burden will shift from the solution of the response matrix equations to their formation. Since the response matrix formation is ideally suited for parallel computation, large gains in computational efficiency can be achieved with larger node sizes. The foregoing calculations represent only one application of the variational nodal method's heterogeneous capabilities. The method may prove valuable for other classes of transport problems, some of which are likely to display quite different tradeoffs between accuracy and refinements of the space-angle approximations.

ACKNOWLEDGMENTS

This work is based, in part, on a dissertation submitted by the first author in partial fulfillment of the PhD requirements at the University of Missouri-Rolla. It was supported by the U.S. Department of Energy under Contract number W-31-109-ENG-38 and by the U.S. Department of Energy Contract number DE-FG07-98ID13632.

REFERENCES

1. M. R. Wagner and K. Koebke, "Progress in Nodal Reactor Analysis," *Proc. Topl. Mtg. Advances in Reactor Computations,* Salt Lake City, Utah, March 28-31, 1983, Vol. II, p. 941, American Nuclear Society (1983).

2. R. D. Lawrence, "Progress in Nodal Methods for the Solution of the Neutron Diffusion and Transport Equations," *Prog. Nucl. Energy*, **17**, 271 (1986).

3. A. Badruzzaman, "Nodal Methods in Transport Theory," *Adv. Nuclear Science and Technology,* Vol. 21, J. Lewins and M. Becker, editors, Plenum Press, New York (1990).

4. G. Palmiotti, E. E. Lewis, C. B. Carrico, "VARIANT: VARIational Anisotropic Nodal Transport for Multidimensional Cartesian and Hexagonal Geometry Calculation," *Argonne National Laboratory* ANL-95/40, 1995.

5. C. B. Carrico, E.E. Lewis and G. Palmiotti, "Three Dimensional Variational Nodal Transport Methods for Cartesian, Triangular and Hexagonal Criticality Calculations," *Nucl. Sci. Eng.* **111**, 168 (1992).

6. E. E. Lewis, C.B. Carrico and G. Palmiotti, "Variational Nodal Formulation for the Spherical Harmonics Equations," *Nucl. Sci. Eng.* **122**, 194 (1996).

7. E. E. Lewis and G. Palmiotti, "Simplified Spherical Harmonics in the Variational Nodal Method," *Nucl. Sci. Eng.* **126**, 48 (1997).

8. E. E. Lewis, G. Palmiotti, and T. Taiwo, "Space-Angle Approximations in the Variational Nodal Method," *Proc. Int. Conf. Mathematics and Computations, Reactor Analysis and Environmental Analysis in Nuclear Applications*, Vol. 1, **827**. September 27-30, Madrid, Spain (1999).

9. G. Ya. Rumyantsev, "Boundary Conditions in the Spherical Harmonic Method," *J. Nucl. Energy*, **16**, 111 (1962).

10. J. N. Reddy, *An Introduction to the Finite Element Method, Second Edition.* Boston, Massachusetts, McGraw-Hill, 1993.

11. M. A. Smith, "Implementation of the Finite Element Approximation in a Nodal Three-Dimensional Transport Program to allow for Explicit Node Geometries," PhD dissertation, University of Missouri-Rolla (2001).

12. E. E. Lewis, G. Palmiotti, T. A. Taiwo, M. A. Smith, & N. Tsoulfanidis, Benchmark Specification for Deterministic 2-D/3-D MOX Fuel Assembly Transport Calculations without Spatial Homogenization (C5G7 MOX), *NEA/NSC/DOC(2001)4*, March 28, 2001.

13. Judith F. Briesmeister and XTM. MCNP^{TM}-A General Monte Carlo N-Particle Transport Code. *LOS ALAMOS National Laboratory LA-12625-M*, March 1997.

14. G. Marleau, A. Hébert, R. Roy, "A User's Guide for DRAGON," Ecole Polytechnique de Montréal, December 1997.

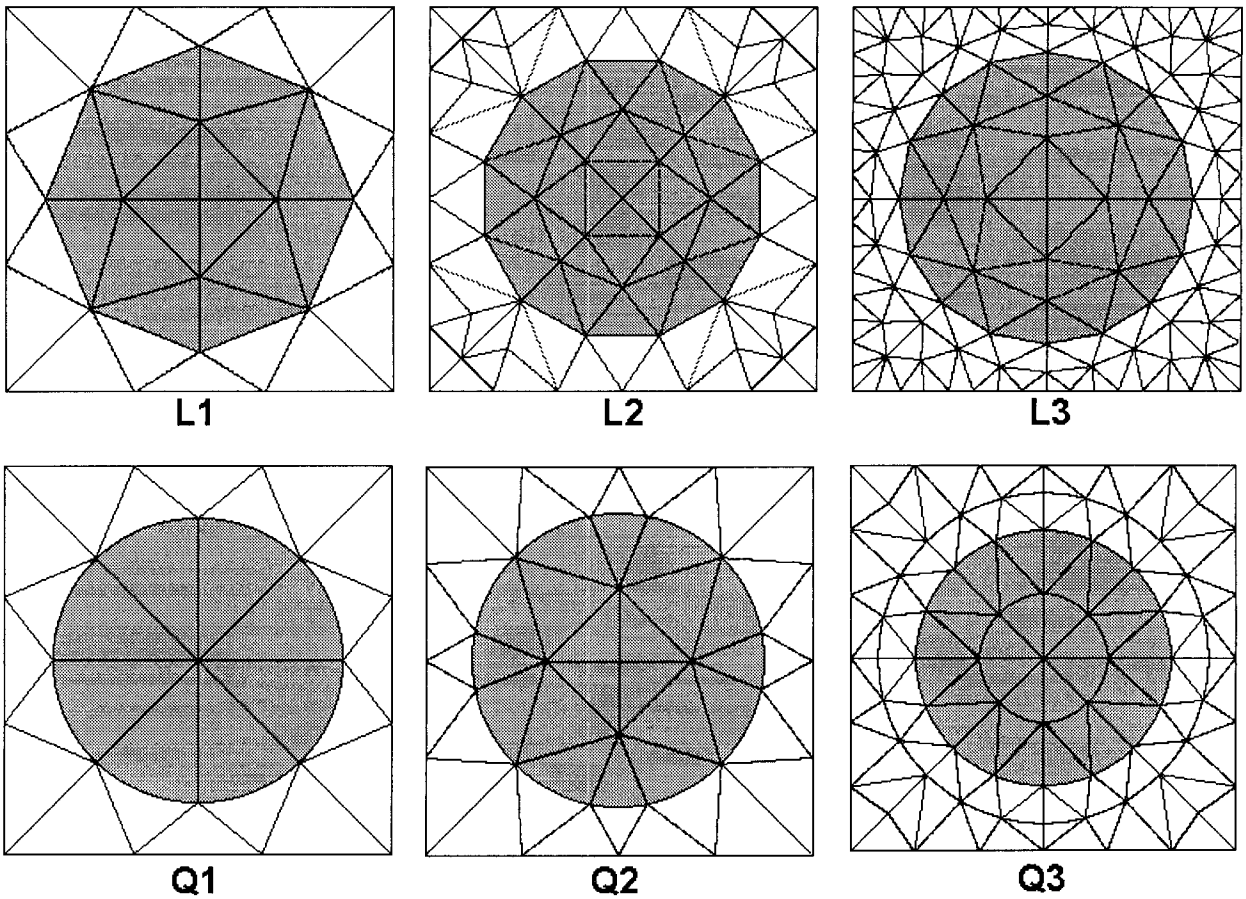

Figure 1. Finite Element Mesh Approximations

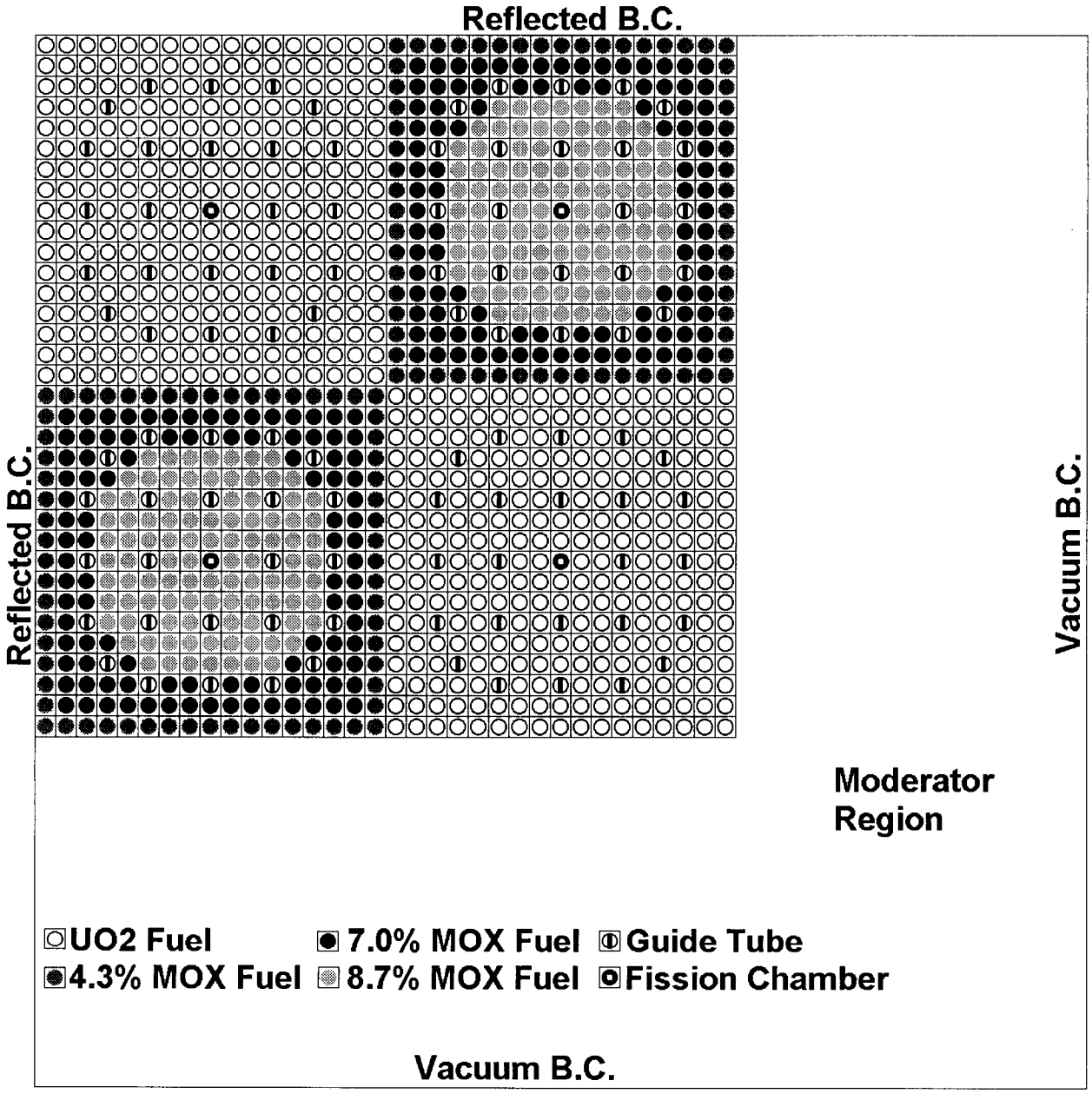

Figure 2. The Benchmark Core Configuration

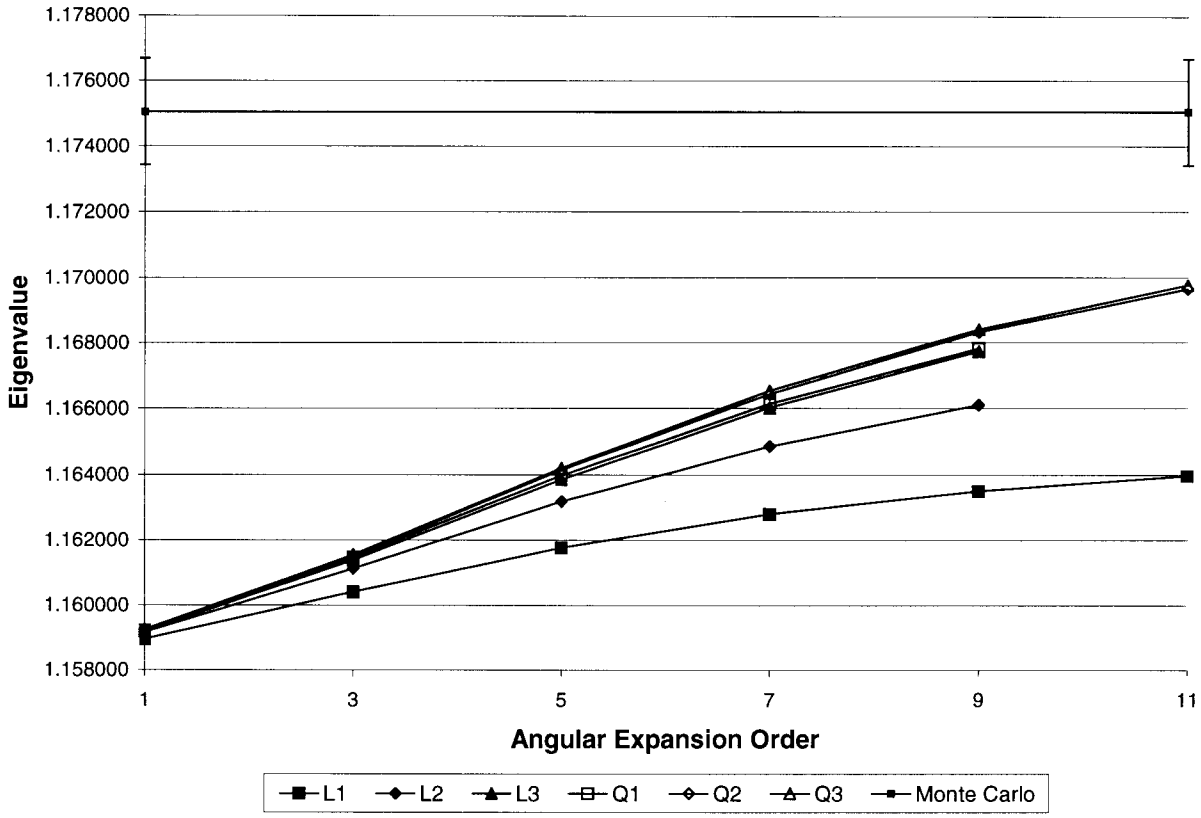

Figure 3. P_N Eigenvalue Convergence Trends for a Single MOX Pin-cell Problem

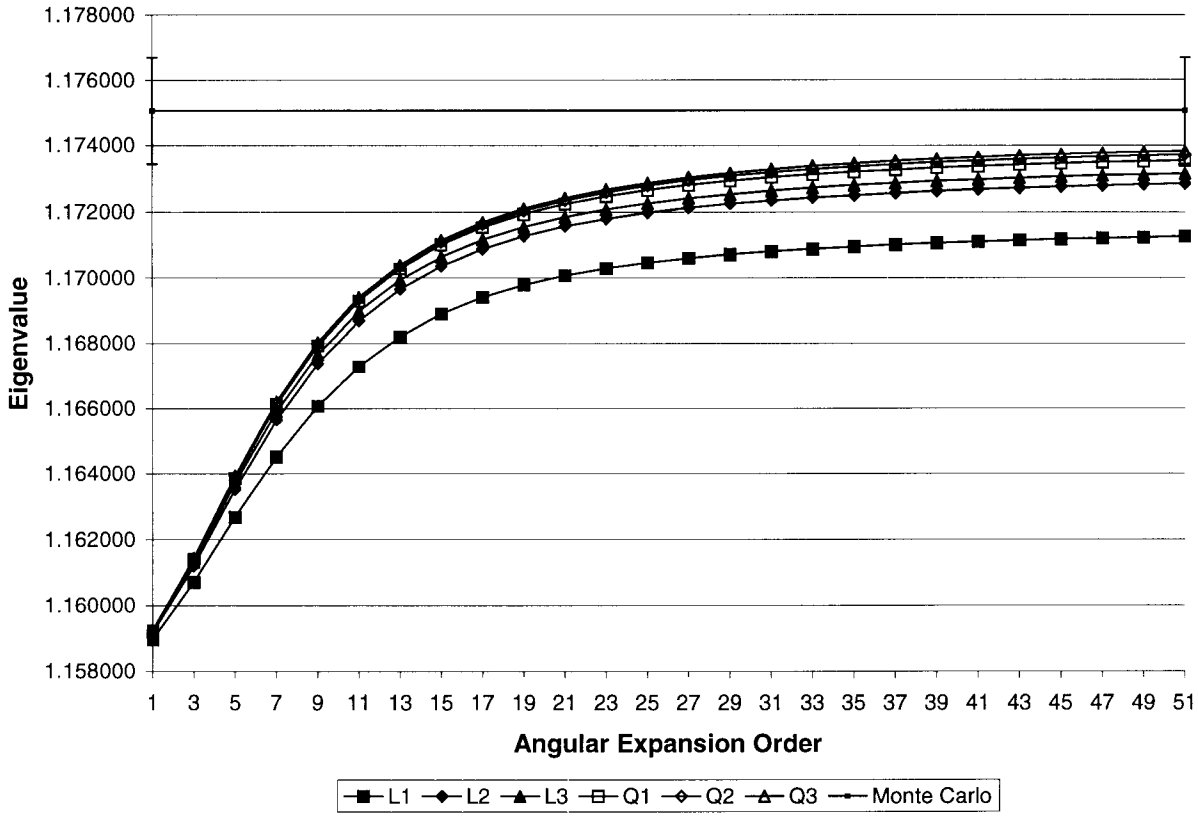

Figure 4. SP_N Eigenvalue Convergence Trend for a Single MOX Pin-cell Problem

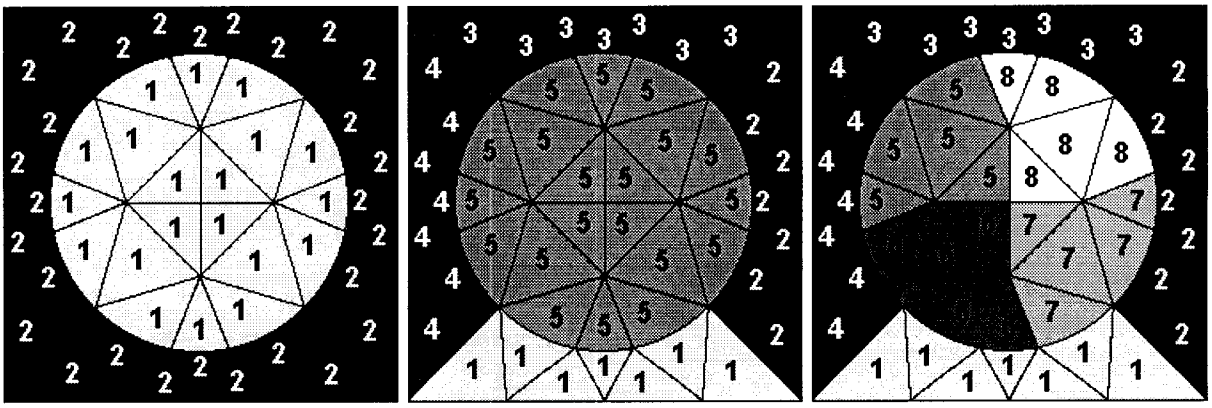

Figure 5. Two, Five, and Eight Lumped Source Representations of the Pin-cell Geometry

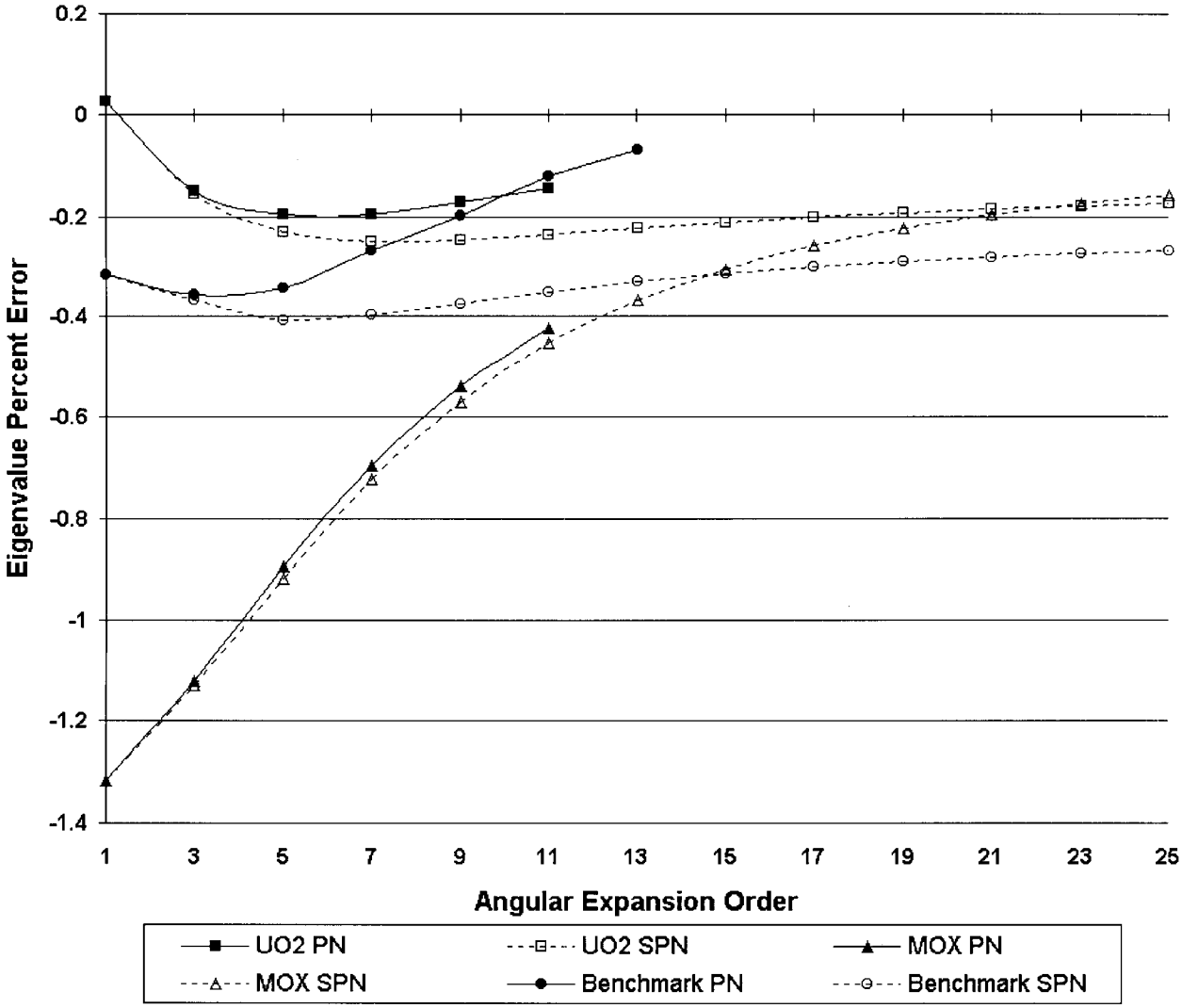

Figure 6. Eigenvalue Percent Errors.

Table I. Percent Errors for the P_N Angular, 8 Lumped Source, Quadratic Lagrange Multiplier Approximation

Angular Order	Eigenvalue	Maximum Pin Power	Maximum	RMS
MCNP Reference	±0.008	0.16	0.58	0.36
P_1	-0.316	0.60	6.44	1.77
P_3	-0.356	0.80	1.92	0.70
P_5	-0.344	0.37	1.21	0.38
P_7	-0.268	-0.02	0.95	0.23
P_9	-0.199	-0.23	0.97	0.27
P_{11}	-0.121	-0.44	1.22	0.39
P_{13}	-0.070	-0.57	1.37	0.47
Homogenized Pin-cell	0.127	1.13	2.41	0.82

Table II. Percent Errors for the SP_N Angular, 8 Lumped Source, Quadratic Lagrange Multiplier Approximation

Angular Order	Eigenvalue	Maximum Pin Power	Maximum	RMS
MCNP Reference	±0.008	0.16	0.58	0.36
SP_1	-0.316	0.60	6.44	1.77
SP_3	-0.367	0.37	3.55	0.85
SP_5	-0.406	-0.24	3.65	0.79
SP_7	-0.397	-0.62	3.59	0.84
SP_9	-0.374	-0.87	3.53	0.92
SP_{11}	-0.351	-1.05	3.48	0.98
SP_{13}	-0.330	-1.16	3.46	1.04
SP_{15}	-0.313	-1.24	3.44	1.08
SP_{17}	-0.300	-1.30	3.44	1.11
SP_{19}	-0.290	-1.35	3.43	1.13
SP_{21}	-0.281	-1.38	3.43	1.15
SP_{23}	-0.274	-1.41	3.44	1.16
SP_{25}	-0.268	-1.43	3.44	1.18

Table III. Percent Errors for the P_N Angular, Consistent Source, Quadratic Lagrange Multiplier Approximation

Angular Order	Eigenvalue	Maximum Pin Power	Maximum	RMS
MCNP Reference	±0.008	0.16	0.58	0.36
P_1	-0.278	0.95	5.90	1.73
P_3	-0.320	1.16	2.03	0.89
P_5	-0.311	0.72	1.44	0.55
P_7	-0.237	0.36	1.04	0.32
P_9	-0.169	0.11	0.75	0.19
P_{11}	-0.092	-0.12	0.64	0.19

Table IV. Percent Errors for the P_N Angular, Consistent Source, Cubic Lagrange Multiplier Approximation

Angular Order	Eigenvalue	Maximum Pin Power	Maximum	RMS
MCNP Reference	±0.008	0.16	0.58	0.36
P_1	-0.278	0.94	5.91	1.73
P_3	-0.287	1.35	2.26	1.02
P_5	-0.286	1.00	1.80	0.76
P_7	-0.250	0.75	1.53	0.59
P_9	-0.205	0.58	1.35	0.47
P_{11}	-0.166	0.47	1.21	0.39
P_{13}	-0.135	0.39	1.12	0.34
SP_{25}	-0.242	-1.13	2.90	0.94